

Atomistic Insights into Interfacial Reactions of FeCr₂O₄ Oxide Films in High-Temperature Water

Haitao Wang^{1,*}, Jiawei Ding^{1,2}, Ruifeng Zhang³, En-Hou Han¹

¹ CAS Key Laboratory of Nuclear Materials and Safety Assessment, Institute of Metal Research, Chinese Academy of Sciences, Shenyang 110016, China

² School of Materials Science and Engineering, University of Science and Technology of China, Shenyang 110016, China

³ School of Materials Science and Engineering, Beihang University, Beijing, 100191, China

*E-mail: htwang@imr.ac.cn

Received: 4 April 2020 / Accepted: 15 June 2020 / Published: 10 August 2020

Interfacial reactions of FeCr₂O₄ oxide films in high-temperature pure water, oxygenated water and hydrogenated water have been investigated by means of ab initio molecular dynamics simulation based on the Born-Oppenheimer scheme. The simulation results show that the surface configuration of FeCr₂O₄ (100) is stable in high-temperature pure water, and the charge transfer of each layer in the oxide film is not significant before and after the film is immersed in water. Dissolved oxygen molecule dissociates spontaneously in high-temperature oxygenated water, and the Cr atoms in the surface layer of the oxide film tend to dissolve in water because of interactions among hydroxyl, oxygen and H₂O molecule. However, dissolved hydrogen molecule does not dissociate in high-temperature hydrogenated water during simulation.

Keywords: Oxide film; High-temperature water; Interfacial reaction; Ab initio molecular dynamics

1. INTRODUCTION

Austenitic stainless steel is of great importance as a structural material in nuclear power plants due to its high corrosion resistance in high-temperature primary water [1-4]. Corrosion in high-temperature primary water is essentially an electrochemical process, while corrosion resistance is mainly dependent on the oxide film formed on the surface during service. Many researchers have found that the characteristics of oxide films formed on stainless steel exposed to high-temperature water are closely related to temperature, solution composition, exposure time, radiation, pre-deformation, surface state, etc [5-10]. In general, the formed oxide film can be divided into a loose outer layer of iron-enriched oxide crystallites and a compact inner layer of nanocrystalline chromium-enriched MCr₂O₄ spinel [11-

14]. It is considered that the formation of the outer layer is a result of the precipitation of dissolved metal ions, while the formation of the inner layer is explained by a solid-state growth mechanism [15]. The preferential dissolution of iron and nickel during passivation and the low diffusivity and solubility of chromium in the lattice lead to an enrichment of chromium in the inner layer.

Although several experiments on the oxide film in high-temperature water have been performed by researchers, very limited knowledge about how the interfacial reaction between the oxide film and high-temperature water evolved is available due to the system complexity and its various nonlinear interactions. A wealth of information about reaction thermodynamics and kinetics would help us understand the electrochemical process on solvated substrate surfaces. In recent years, the full ab initio molecular dynamics simulations of solid/liquid interfaces with the Born-Oppenheimer scheme have become feasible because of the development of microscopic theories and computational facilities [16-20]. Born-Oppenheimer molecular dynamics separates the motion of atomic nuclei and electrons and solves the electron distributions for all atoms in the system to find the local energy minima of a Born-Oppenheimer surface. Subsequently, the force on each atom can be calculated based on the results of electron distributions and then the atomic motion is determined according to Newton's law. This approach allows direct observation of some kinetic processes at an atomic scale, which is extremely difficult to achieve through traditional experimental techniques. Costa et al. studied the reactivity of water on Cr_2O_3 (0001) surfaces with different degrees of water coverage at ambient temperature by Born-Oppenheimer molecular dynamics [21]. Sebbari et al. investigated the effect of hydrogen bonds and temperature on water adsorption on TiO_2 (110) surfaces by the Born-Oppenheimer approach [22]. We have also studied the interactions between the outer oxide film of Fe_3O_4 (111) and high-temperature pure water based on this approach [23]. However, an electrolyte can be transported to the inner oxide film surface across the loose outer oxide film. At this time, the inner oxide film plays a key role in corrosion resistance in high-temperature water. Therefore, the objectives of the current work are to investigate the interfacial reactions of a typical inner oxide film of FeCr_2O_4 spinel in 320°C high-temperature pure water, oxygenated water and hydrogenated water through Born-Oppenheimer molecular dynamics, and to elucidate their microscopic kinetic mechanisms at the electronic/atomic level.

2. COMPUTATIONAL METHODS

We performed Born-Oppenheimer molecular dynamics simulations within the framework of density functional theory, as implemented in the Vienna ab initio simulation package (VASP) [24]. The FeCr_2O_4 oxide surface was modelled using a slab geometry with periodic boundary conditions corresponding to the (100) Miller plane. The slab consisted of eleven layers, containing 10 Fe atoms, 24 Cr atoms and 48 O atoms. A vacuum layer of 10 Å along the z-direction perpendicular to the surface was used to avoid the interactions between the repeated slabs. The whole simulation unit is an $8.1224 \times 8.1224 \times 20.2409$ Å³ supercell. Seventeen H_2O molecules were placed in the vacuum layer according to the density of high-temperature water of $\rho = 0.76$ g/cm³, and the hydrogen bond interactions among H_2O molecules were fully optimized to minimize close contacts [25]. The middle three atomic layers in the oxide film were fixed at the bulk interatomic distance whereas the rest of the atomic layers

were allowed to relax.

Blöchl's all-electron projector augmented wave (PAW) method constructed by Kresse and Joubert [26] was employed to address the effect of core electrons on the valence density. The generalized gradient approximation (GGA) functional developed by Perdew, Burke, and Ernzerhof (PBE) [27] was used to simulate the electron exchange and correlation energy, which is reliable in describing the solid surface properties and bulk properties of water as well as hydrogen bonds. The Fe, Cr, O and H pseudopotentials have valence states of $3d^64s^2$, $3d^54s^1$, $2s^22p^4$ and $1s^1$, respectively. All calculations were performed with spin polarization. The Monkhorst-Pack scheme was used for k-point sampling, and Brillouin-zone integrations were carried out with only gamma point for the large unit supercell. The first-order Methfessel-Paxton method was chosen with a smearing width of 0.2 eV to obtain accurate forces. A kinetic energy cut-off of 400 eV was used for the plane wave expansion of the electron wavefunction. The convergence calculations were carried out until the forces acting on all of the atoms were less than 0.05 eV/Å, with convergence at a total energy of 10^{-4} eV. During the simulation, a Verlet algorithm was utilized to integrate the motion equations. The volume and temperature were kept constant (NVT ensemble), with the temperature controlled by the velocity scaling method. The temperature was set to 320°C, which is the temperature in a pressurized water reactor. The total number of simulation steps was 3000, and the duration of each step was 1 fs.

3. RESULTS AND DISCUSSION

3.1 Interfacial reactions in high-temperature pure water

The surface morphologies of $\text{FeCr}_2\text{O}_4(100)$ in high-temperature pure water in the initial state and after a 3 ps calculation are displayed in Figure 1. The surface configuration of $\text{FeCr}_2\text{O}_4(100)$ is very stable in high-temperature pure water after the 3 ps calculation. Six H_2O molecules adsorb atop Cr atoms in the surface layer, with the O-H bonds pointing away from the surface. Figure 2(a) shows the trajectories of three typical Cr-H₂O bonds. The adsorption time of the H_2O molecules on the surface varies from 20 fs to 2400 fs. After adsorption, the bond lengths in the H_2O molecules fluctuate around the equilibrium lengths, which are 2.18 Å, 2.16 Å, and 2.17 Å, similar to the literature value of 2.1 Å [21]. It can be observed in Figure 2(b) that one OH bond in the H_2O molecule in the W1 location in Figure 1(a) always maintains its equilibrium bond length of 1.0 Å, in agreement with the literature value of 0.97 Å [28]. Nevertheless, the bond length of another OH in this H_2O molecule increases rapidly at approximately 2500 fs, which suggests that the H_2O molecule is dissociated.

The OH moiety of the dissociated H_2O forms a bond with the Cr atom on the surface to form hydroxide, as shown in the P1 location in Figure 1(b). However, Figure 2(c) shows that the Cr-OH bonds formed before the hydroxide was produced. This indicates that the H_2O molecule first adsorbs on this Cr atom, and then dissociation occurs.

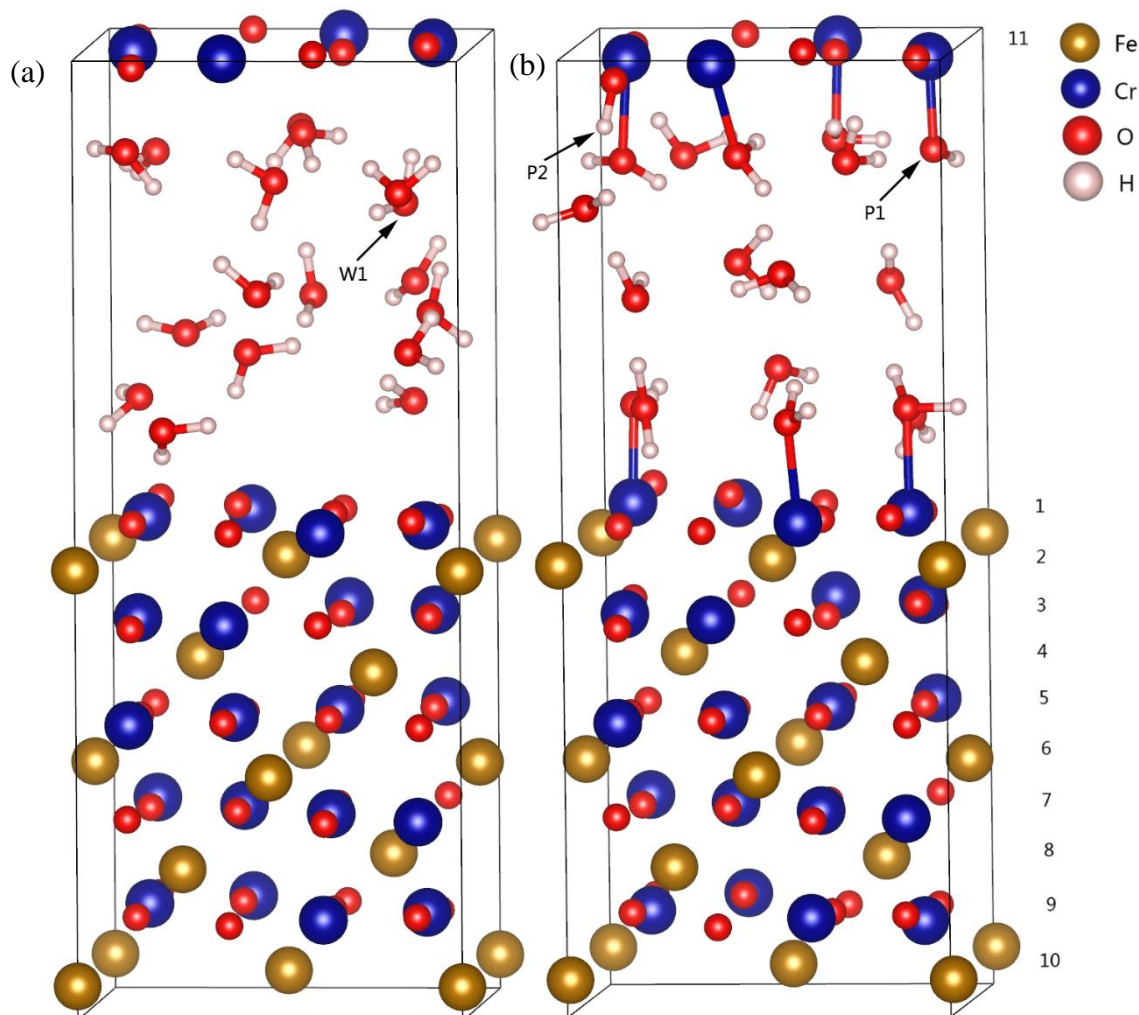


Figure 1. The surface morphologies of $\text{FeCr}_2\text{O}_4(100)$ in high-temperature pure water, (a) in the initial state and (b) after a 3 ps calculation.

Bonding in the form of Cr-H₂O occurs with an average bond length of 2.18 Å before the H₂O molecule is dissociated at 2500 fs, and the bond length is decreased to 2.03 Å after dissociation of the H₂O molecule, which is similar to the literature value of 1.95 Å for Cr-OH hydroxide [29]. To analyse the interaction mechanism, the partial density of states (PDOS) is shown in Figure 3. The valence electrons of the Cr atom mostly occupy the 3d orbital. The electronic states are highly localized around the Fermi level of 3.11 eV, while the valence electrons of H and O atoms mostly occupy 2p and 1s orbitals, respectively. There are significant overlapping regions in the range of -7.89 eV to -2.34 eV for Cr, O and H atoms. This demonstrates that hybridization between the chromium 3d orbital and the oxygen 2p orbital occurs. The electronic states of the H and O atoms traverse the Fermi level because of their orbital hybridization with Cr metal atoms. It can be seen in Figure 1(b) that the H from the dissociated H₂O forms a hydroxyl moiety by combining with the O atom on the FeCr_2O_4 surface, labelled P2 in the figure, and this O-H bonding occurs almost simultaneously with Cr-OH bonding, as shown in Figure 2(d).

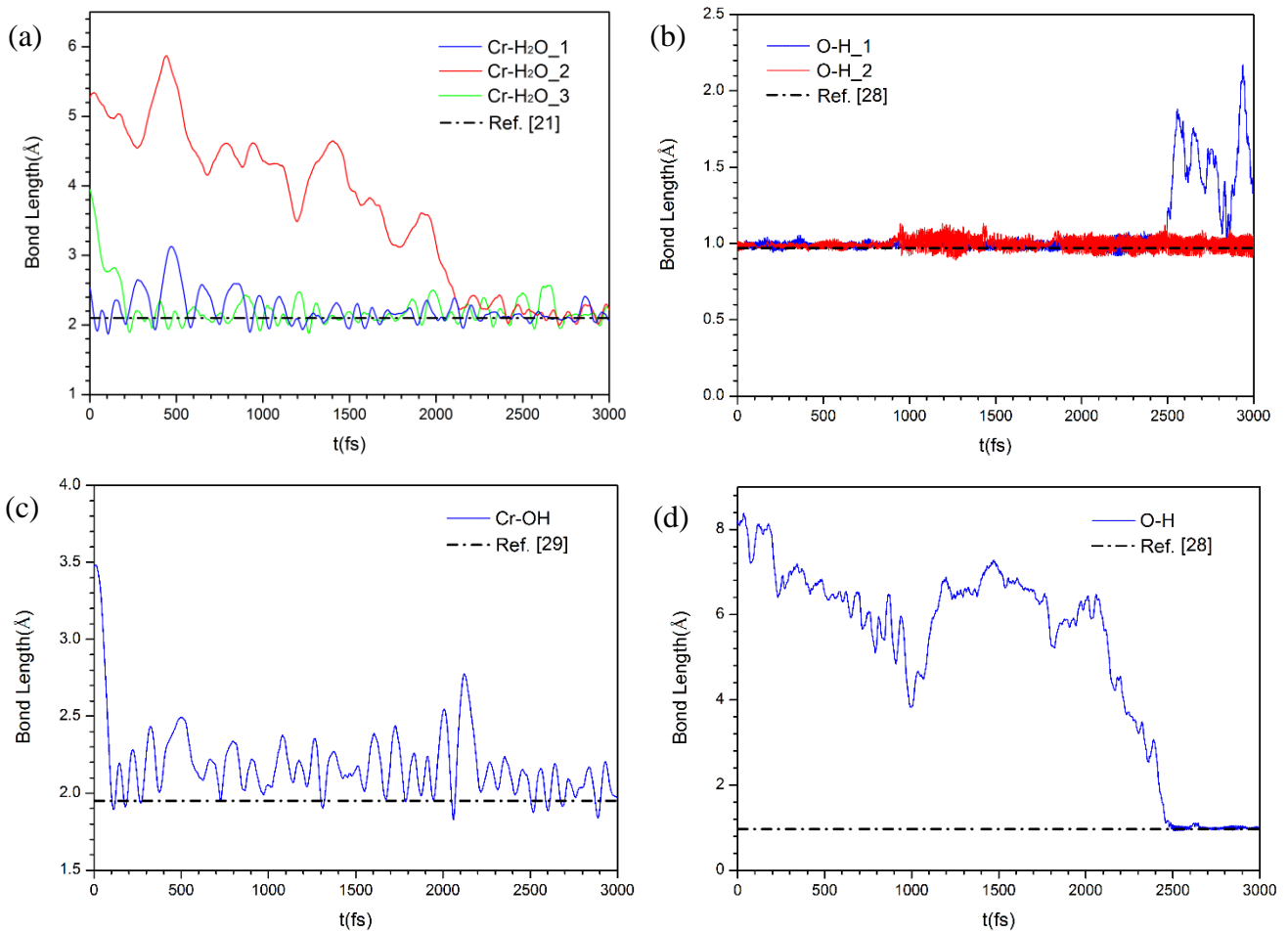
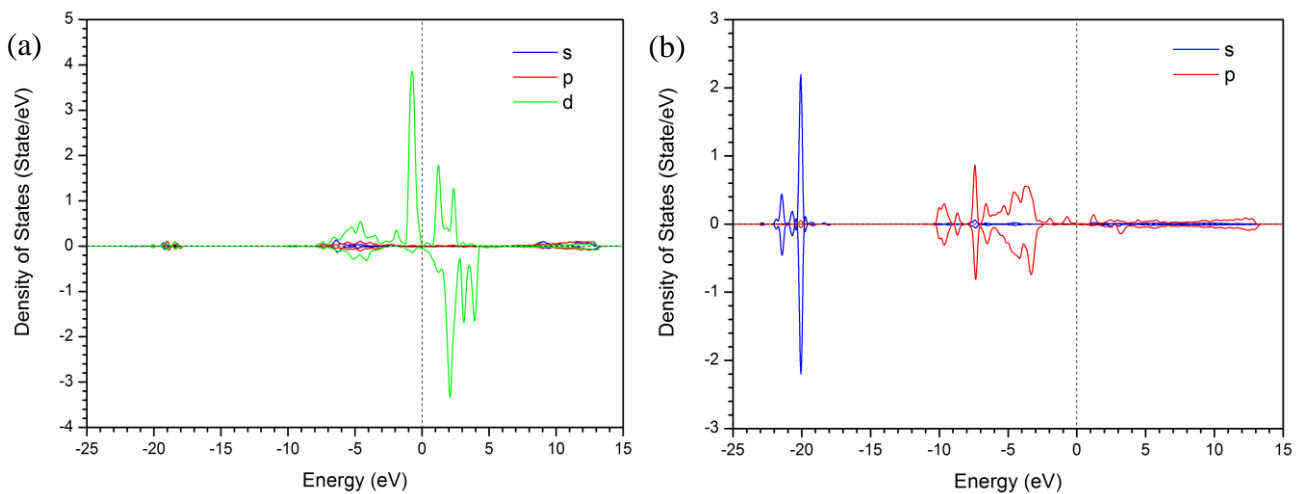


Figure 2. The trajectories for (a) adsorption of H₂O molecules on the Cr atoms, (b) dissociation of H₂O molecule in the W1 location in Figure 1a, (c) Cr-OH bonding in the P1 location in Figure 1b, (e) O-H bonding in the P2 location in Figure 1b.



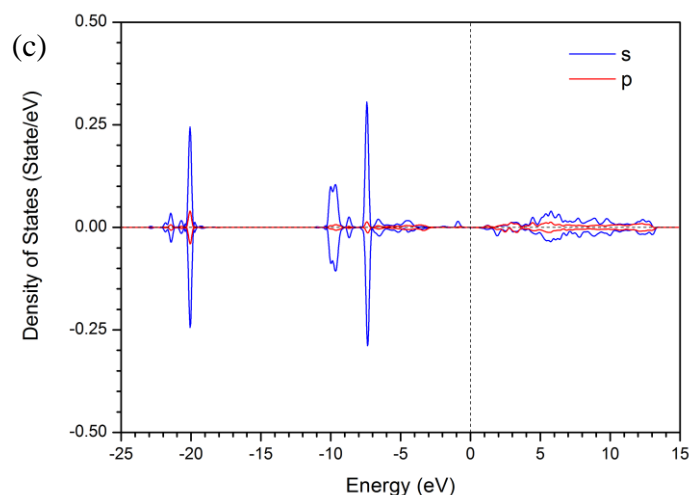


Figure 3. The partial density of states (PDOS) for (a) Cr atom, (b) O atom and (c) H atom in the P1 location in Figure 1b. The Fermi Level is 3.11 eV.

We further analyse the interfacial charge transfer of $\text{FeCr}_2\text{O}_4(100)$ in high-temperature pure water by semiquantitative Bader charge analysis, in which the total density is divided into atoms in the system with a zero flux surface. Figure 4(a) demonstrates the charge transfer of each atom of $\text{FeCr}_2\text{O}_4(100)$ in high-temperature pure water. The charge transfer is not significant before and after the oxide film is immersed in the water due to the weak interaction between the oxide film and water. The Fe and Cr atoms in the oxide film are electron donors, donating 1.36e and 1.56e, respectively, while the O atoms in the oxide film are electron acceptors, accepting 1.06e. The electronegativity of the Cr atom is lower than that of the Fe atom, with values of 1.66 and 1.83 respectively; therefore, the Cr atom donates more electrons than the Fe atom. The O atoms in the H_2O molecules accept approximately 1.24e, which is higher than that of O atoms in the oxide film, while the H atoms donate approximately about 0.62e. The errors between our calculation results and the literature values [30] are less than 10%, showing that the reliability of the calculation is very high. The charge transfer of each layer of $\text{FeCr}_2\text{O}_4(100)$ in high-temperature pure water is presented in Figure 4(b). The $\text{FeCr}_2\text{O}_4(100)$ oxide film has a heterogeneous charge distribution. The layers composed of Cr atoms and O atoms are negatively charged, while the layers composed of Fe atoms are positively charged. Surface layer 1 and layer 11 gain fewer electrons than other inner layers of the same kind because of the existence of a surface state. However, the charge transfer of each layer is not significant before and after immersion, which is similar to those for each atom.

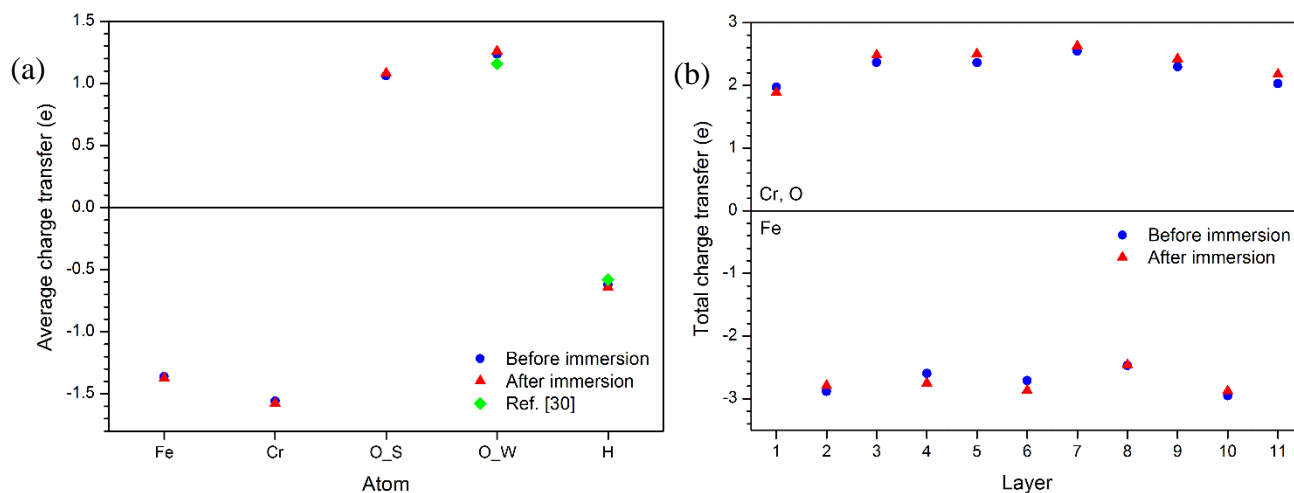


Figure 4. The charge transfer of (a) each atom and (b) each layer of $\text{FeCr}_2\text{O}_4(100)$ in high-temperature pure water.

3.2. The dissolved oxygen and hydrogen additions

The radiolysis of primary water in nuclear plants can produce dissolved oxygen; in addition, supplemental water also takes dissolved oxygen into the primary loop. It is generally accepted that dissolved oxygen can enhance corrosion damage [31]. However, the microscopic features of dissolved oxygen molecules in high-temperature water are not well understood. In this work, we added one dissolved oxygen molecule to high-temperature water, labelled DO in Figure 5(a). During a 3 ps calculation, the dissociation of the DO molecule occurs spontaneously, as shown in Figure 5(b). Figure 6(a) shows that the O-O bond fluctuates at the equilibrium position with an average value of 1.44 Å before approximately 1.1 ps, which is similar to the literature value of 1.47 Å [32]; subsequently, the O-O bond length increases rapidly, and the O-O bond is broken. After dissociation of the DO molecule, four Cr-OH bonds and one Cr-O bond are formed on the $\text{FeCr}_2\text{O}_4(100)$ surface, and surface reconstruction obviously occurs, as shown in Figure 5(b), which is different from the process in high-temperature pure water in Figure 1(b). The two Cr atoms in surface layer 1 and layer 11 tend to dissolve in high-temperature water as a result of interactions among hydroxyl, oxygen and H_2O molecule. The typical Cr-OH bonding and Cr-O bonding for these two Cr atoms are displayed in Figure 6. It can be found in Figure 6(b) that the Cr-OH bonding in the P1 and P2 locations in Figure 5(b) occurs at approximately 1300 fs and 1600 ps, respectively, later than the dissociation time of the O-O bond in the DO molecule. In fact, after the O-O bond in the DO molecule is broken, the dissociated O atoms capture the H atoms in H_2O molecules continually induce the dissociation of H_2O molecules. Cr-OH bonding on the $\text{FeCr}_2\text{O}_4(100)$ surface results from the dissociated H_2O molecules, while the two O atoms in the DO molecule form new H_2O molecules. Figure 6(c) shows that the bonding time of Cr-O in the P3 location in Figure 5(b) is approximately 300 fs, which is much earlier than the dissociation time of the O-O bond in the DO molecule. Similar to Cr-OH bonding in Figure 2(c), the Cr- H_2O bond is initially formed in the P3 location; subsequently, successive reactions caused by the dissociation of the DO molecule capture H atoms in this bond. This leads to the transformation of Cr- H_2O bonds into Cr-O bonds.

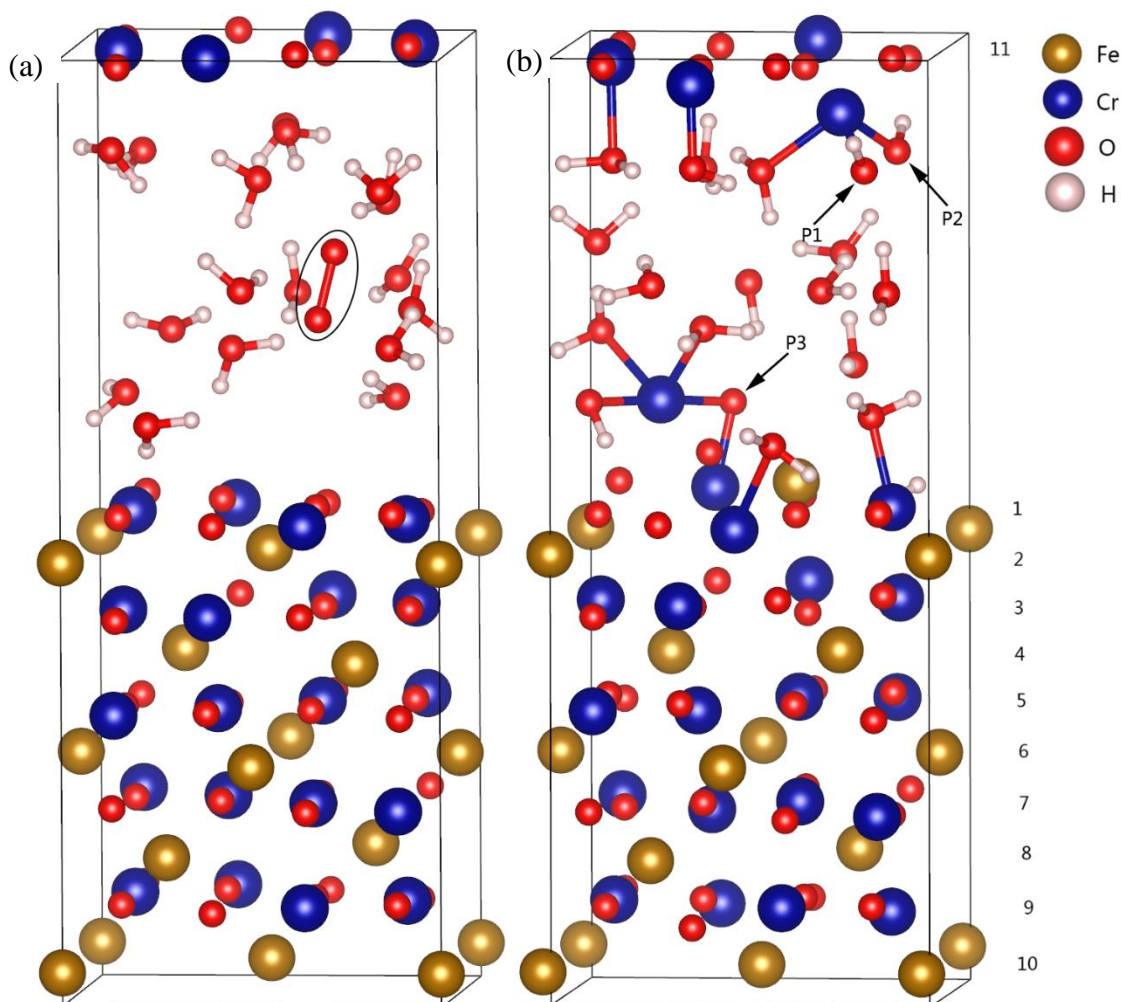
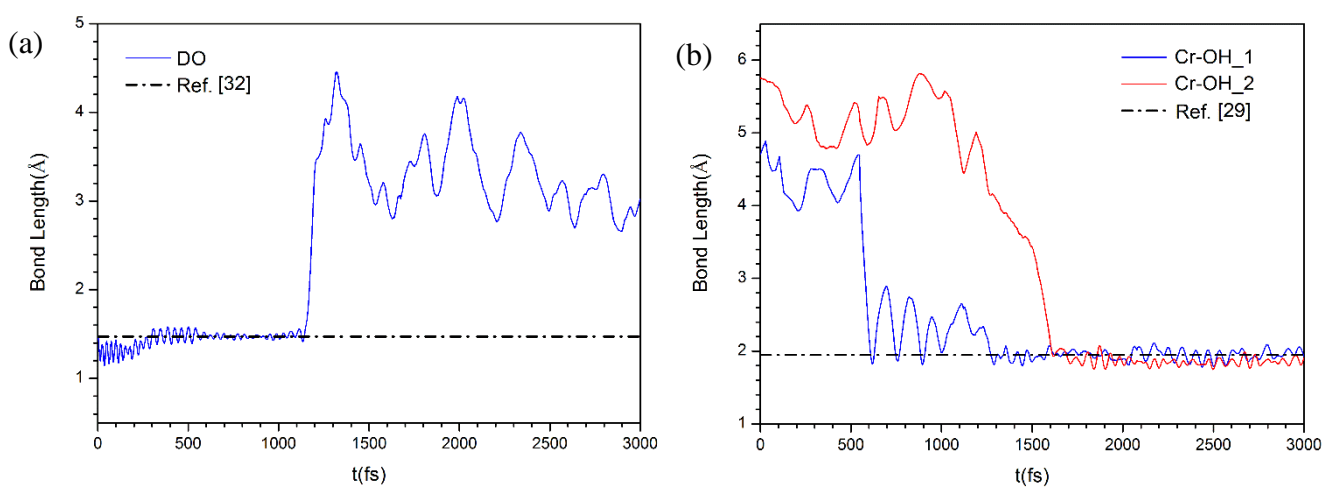


Figure 5. The surface morphologies of $\text{FeCr}_2\text{O}_4(100)$ in high-temperature oxygenated water, (a) in the initial state and (b) after a 3 ps calculation.



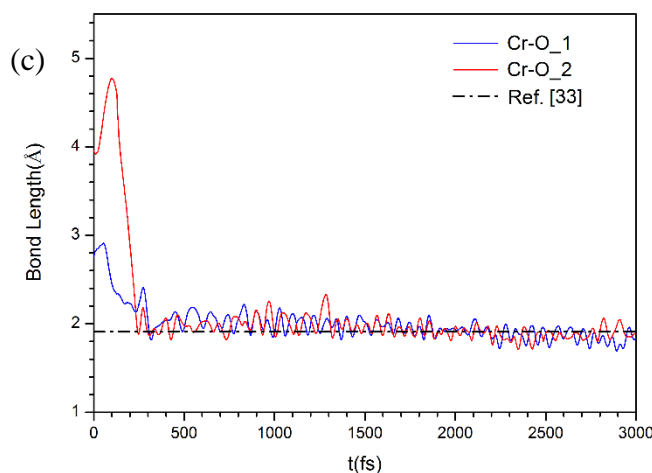


Figure 6. The trajectories for (a) dissociation of dissolved oxygen molecule in the DO location in Figure 5a, (b) Cr-OH bonding in the P1 and P2 locations in Figure 5b, (c) Cr-O bonding in the P3 location in Figure 5b.

The charge transfer of each layer of $\text{FeCr}_2\text{O}_4(100)$ in high-temperature oxygenated water are shown in Figure 7. After the oxide film is immersed in high-temperature water, both surface layers donate a portion of their valence electrons; surface layer 1 donates more electrons than surface layer 11, with values of $0.97e$ and $0.42e$, respectively. As mentioned above, hydroxide is produced on surface layer 11. Nevertheless, the oxide is also formed on surface layer 1. The strong interactions between the Cr atom and the O atoms on surface layer 1 lead to more significant charge transfer than those on surface layer 11. The inner layers composed of Fe undergo little charge transfer before and after immersion, while the inner layers composed of Cr and O atoms gain some electrons. It is noted that most of the electrons donated from the surface layers of the $\text{FeCr}_2\text{O}_4(100)$ oxide film come into the solution across the oxide/electrolyte interface, and only a fraction of the electrons transfer to the inner layers of the $\text{FeCr}_2\text{O}_4(100)$ oxide film.

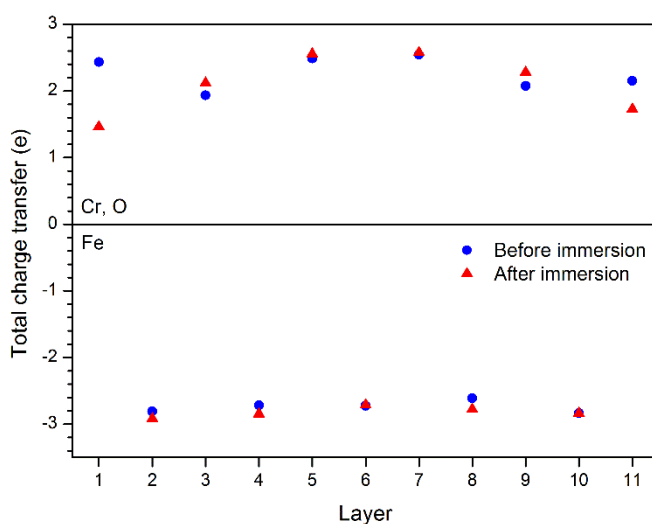


Figure 7. The charge transfer of each layer of $\text{FeCr}_2\text{O}_4(100)$ in high-temperature oxygenated water.

Figure 8 shows the surface morphologies of $\text{FeCr}_2\text{O}_4(100)$ in high-temperature hydrogenated

water in the initial state and after a 3 ps calculation. Hydrogen addition to primary water in nuclear plants can reduce the corrosion potential of materials and control the radiolysis of the reactor coolant. Figure 8(b) shows that the dissolved hydrogen molecule is still not dissociated after the 3 ps calculation. Figure 9 demonstrates the trajectory for dissolved hydrogen molecule in the DH location in Figure 8. The H-H bond length always fluctuates around the equilibrium position, with an average value of 0.76 Å, similar to the literature value of 0.74 Å [34], showing that the H-H bond is not broken during the simulation. The bond energy of the H-H is slightly lower than that of the O-O bond in the gas phase at room temperature, with values of 436 kJ/mol and 497 kJ/mol respectively [35]. However, the DH molecule has better stability in high-temperature water than the DO molecule under the interaction between solvation and temperature for the $\text{FeCr}_2\text{O}_4(100)$ surface.

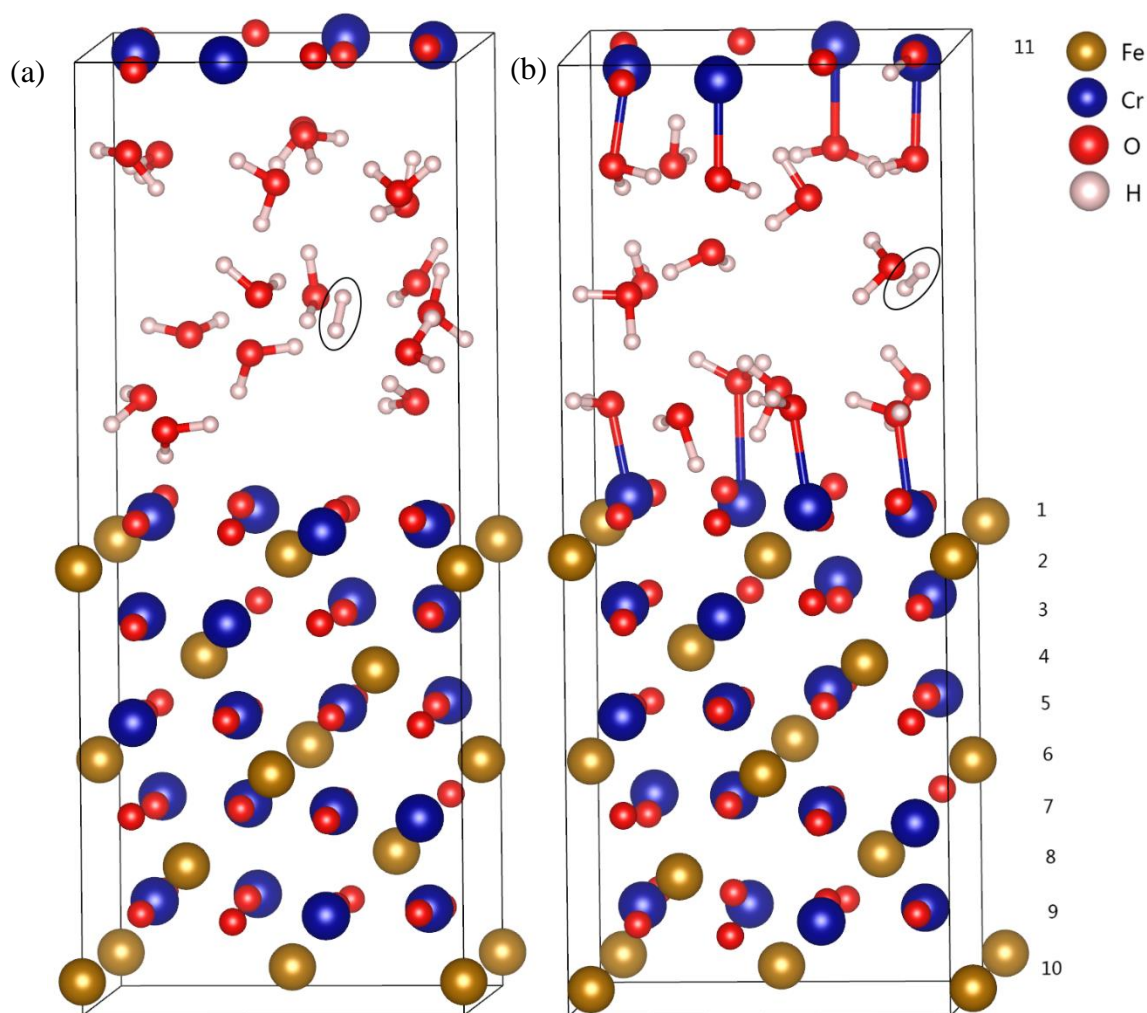


Figure 8. The surface morphologies of $\text{FeCr}_2\text{O}_4(100)$ in high-temperature hydrogenated water, (a) in the initial state and (b) after a 3 ps calculation.

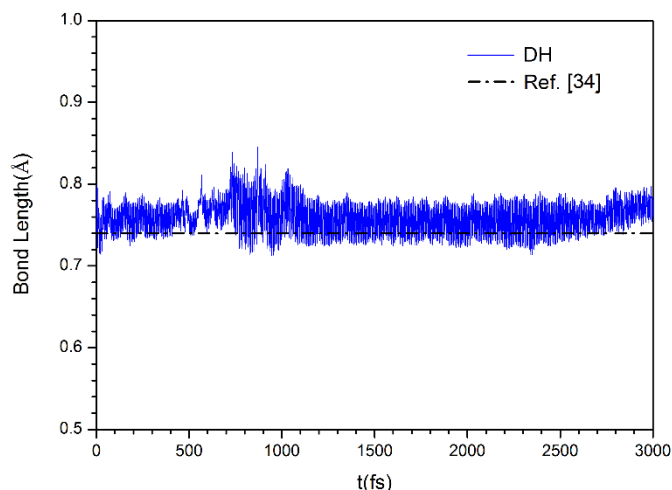


Figure 9. The trajectory for dissolved hydrogen molecule in the DH location in Figure 8.

4. CONCLUSIONS

A Born-Oppenheimer molecular dynamics simulation was used to investigate the interfacial reactions of an FeCr_2O_4 (100) oxide film in high-temperature water. The surface configuration of the oxide film is stable in high-temperature pure water after a 3 ps calculation. Six H_2O molecules adsorb atop Cr atoms in the surface layer of the oxide film, and one H_2O molecule is dissociated. The dissociated OH forms a bond with the Cr atom on the surface to form hydroxide, and hybridization between the Cr 3d orbital and the O 2p orbital occurs, while the dissociated H forms a hydroxyl moiety by combining with an O atom on the surface. The FeCr_2O_4 (100) oxide film has a heterogeneous charge distribution. The charge transfer of each layer is not significant before and after immersion. After a 3 ps calculation, the dissociation of dissolved oxygen molecule in high-temperature pure water occurs spontaneously. Four Cr-OH bonds and one Cr-O bond are formed on the surface, and surface reconstruction obviously occurs. The two Cr atoms in the surface layers tend to dissolve in the high-temperature water because of interactions among hydroxyl, oxygen and H_2O molecule. There is significant charge transfer behaviour at the oxide film/solution interface. The dissolved hydrogen molecule in high-temperature pure water is still not dissociated after the 3 ps calculation.

ACKNOWLEDGMENTS

This work was supported by the National Key Research and Development Program of China (Grant No. 2017YFB0702100) and Key Research Program of Frontier Sciences, CAS (QYZDY-SSW-JSC012).

References

1. L.T. Chang, M.G. Burke and F. Scenini, *Corros. Sci.*, 138 (2018) 54
2. Y.L. Han, J.N. Mei, Q.J. Peng, E.-H. Han and W. Ke, *Corros. Sci.*, 112 (2016) 625
3. Z.Y. Zhang, J.B. Tan, X.Q. Wu, E.-H. Han, W. Ke and J.C. Rao, *J. Nucl. Mater.*, 518 (2019) 21
4. J.J. Chen, Z.P. Lu, Q. Xiao, X.K. Ru, G.D. Han, Z. Chen, B.X. Zhou and T. Shoji, *J. Nucl. Mater.*, 472 (2016) 1

5. X.H. Liu, E.-H. Han and X.Q. Wu, *Corros. Sci.*, 78 (2014) 200
6. Q. Xiao, Z.P. Lu, J.J. Chen, J.R. Ma, Q. Xiong, H.J. Li, J. Xu and T. Shoji, *J. Nucl. Mater.*, 518 (2019) 357
7. W.J. Kuang, X.Q. Wu and E.-H. Han, *Corros. Sci.*, 63 (2012) 259
8. R.D. Hanbury and G.S. Was, *Corros. Sci.*, 157 (2019) 305
9. J.L. Lv, T.X. Liang and H.Y. Luo, *Nucl. Eng. Des.*, 309 (2016) 1
10. J. Xu, X.Q. Wu and E.-H. Han, *Electrochim. Acta*, 71 (2012) 219
11. S.E. Ziemniak and M. Hanson, *Corros. Sci.*, 44 (2002) 2209
12. P. Kritzer, N. Boukis and E. Dinjus, *Corrosion*, 56 (2000) 1093
13. D.X. Chen, X.Q. Wu, E.-H. Han and H.T. Sun, *Corrosion*, 71 (2015) 1213
14. Z.Y. Li, Z.B. Cai, T. Zhou, X.Y. Shen and G.H. Xue, *Mater. Chem. Phys.*, 222 (2019) 267
15. B. Stellwag, *Corros. Sci.*, 40 (1998) 337
16. D.R. Yarkony, *J. Phys. Chem.*, 100 (1996) 18612
17. S. Izvekov, A. Mazzolo, K. VanOpdorp and G.A. Voth, *J. Chem. Phys.*, 114 (2001) 3248
18. P. Vassilev, R.A. van Santen and M.T.M. Koper, *J. Chem. Phys.*, 122 (2005) 054701
19. S. Schnur and A. Groß, *New J. Phys.*, 11 (2009) 125003
20. T. Ikeshoji, M. Otani, I. Hamada and Y. Okamoto, *Phys. Chem. Chem. Phys.*, 13 (2011) 20223
21. D. Costa, K. Sharkas, M. M. Islam and P. Marcus, *Surf. Sci.*, 603 (2009) 2484
22. K. Sebbari, C. Domain, J. Roques, H. Perro, E. Simoni and H. Catalette, *Surf. Sci.*, 605 (2011) 1275
23. H.T. Wang, X.F. Sun and E.-H. Han, *Int. J. Electrochem. Sci.*, 13 (2018) 2430
24. G. Kresse and J. Furthmüller, *Phys. Rev. B*, 54 (1996) 11169
25. H.T. Wang and E.-H. Han, *Comp. Mater. Sci.*, 149 (2018) 143
26. G. Kresse and D. Joubert, *Phys. Rev. B*, 59 (1999) 1758
27. J.P. Perdew, K. Burke and M. Ernzerhof, *Phys. Rev. Lett.*, 77 (1996) 3865
28. S.L. Liu, X.X. Tian, T. Wang, X.D. Wen, Y.W. Li, J.G. Wang and H.J. Jiao, *Phys. Chem. Chem. Phys.*, 17 (2015) 8811
29. H.G. Visser, W. Purcell and S.S. Basson, *Polyhedron*, 18 (1999) 2795
30. G. Henkelman, A. Arnaldsson and H. Jonsson, *Comput. Mater. Sci.*, 36 (2006) 354
31. F. Arjmand, L.F. Zhang and J.M. Wang, *Nucl. Eng. Des.*, 322 (2017) 215
32. H. Lebel, C. Ladjel, F. Belangergaripey and F. Schaper, *J. Organomet. Chem.*, 693 (2008) 2645
33. W. Wei, Y. Dai, H. Jin and B.B. Huang, *J. Phys. D: Appl. Phys.*, 42 (2009) 055401
34. H. Yang and J.L. Whitten, *J. Chem. Phys.*, 98 (1993) 5039
35. D.R. Lide, *CRC handbook of chemistry and physics*, 83rd ed., CRC Press, New York, 2002